Langmuir

Article

pubs.acs.org/Langmuir

Analysis of Lipid Phase Behavior and Protein Conformational Changes in Nanolipoprotein Particles upon Entrapment in Sol–Gel-Derived Silica

Wade F. Zeno,[†] Silvia Hilt,[‡] Kannan K. Aravagiri,[†] Subhash H. Risbud,[†] John C. Voss,[‡] Atul N. Parikh,[†] and Marjorie L. Longo*[,†]

[†]Department of Chemical Engineering and Materials Science and [‡]Department of Biochemistry and Molecular Medicine, University of California Davis, Davis, California 95616, United States

Supporting Information

ABSTRACT: The entrapment of nanolipoprotein particles (NLPs) and liposomes in transparent, nanoporous silica gel derived from the precursor tetramethylorthosilicate was investigated. NLPs are discoidal patches of lipid bilayer that are belted by amphiphilic scaffold proteins and have an average thickness of 5 nm. The NLPs in this work had a diameter of roughly 15 nm and utilized membrane scaffold protein (MSP), a genetically altered variant of apolipoprotein A-I. Liposomes have previously been examined inside of silica sol–gels and have been shown to exhibit instability. This is attributed to their size (~150 nm) and altered structure and constrained lipid dynamics upon entrapment within the nanometer-scale pores (5–50 nm) of the silica gel. By contrast, the dimensional match of NLPs with the intrinsic pore sizes of silica gel opens the possibility for their entrapment without disruption. Here we demonstrate that NLPs are more compatible with the nanometer-scale size of the porous environment by analysis of lipid phase behavior via fluorescence anisotropy and analysis of scaffold protein secondary structure via circular dichroism spectroscopy. Our results showed that the lipid phase behavior of NLPs entrapped inside of silica gel display closer resemblance to its solution behavior, more so than liposomes, and that the MSP in the NLPs maintain the high degree of α-helix secondary structure associated with functional protein–lipid interactions after entrapment. We also examined the effects of residual methanol on lipid phase behavior and the size of NLPs and found that it exerts different influences in solution and in silica gel; unlike in free solution, silica entrapment may be inhibiting NLP size increase and/or aggregation. These findings set precedence for a bioinorganic hybrid nanomaterial that could incorporate functional integral membrane proteins.

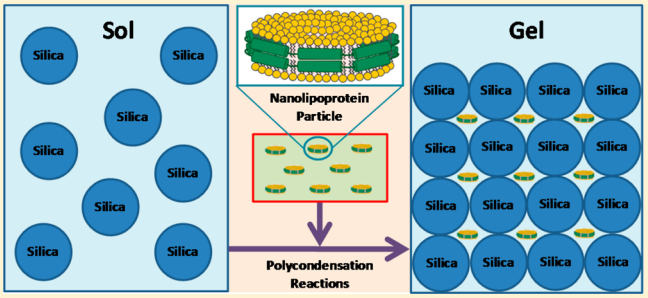

INTRODUCTION

Over the past several decades, the entrapment of proteins in transparent, mesoporous silica has been of significant interest to scientists and engineers spanning a broad spectrum of disciplines.[1−3] In more recent history, integral membrane proteins (IMPs) have been of particular interest for entrapment in sol–gel-derived silica due to their differing functionalities that can be exploited to tailor these systems for accommodating various applications, such as biosensing, affinity chromatography, high-throughput drug screening, and bioreaction engineering.[4−7] IMPs contain both hydrophobic and hydrophilic amino acid residues; thus, they are either partially or completely embedded within amphiphilic lipid bilayers of cell membranes. This allows the IMPs to maintain their proper tertiary conformation. The necessity of lipid bilayers for proper IMP functionality requires an entrapment system that minimally modulates the physical and structural properties of the lipid bilayers; direct modification of the lipid bilayer structures would adversely affect protein conformation within it.[8−11] Therefore, the investigation of the stability of lipid-bilayer-derived structures (i.e. nanolipoprotein particles and liposomes) entrapped within silica gel is essential to the development of viable, efficient IMP-derived bioinorganic hybrid materials.

During the 1990s, research groups of Bright, Friedman, Kostic, and Brennan examined the properties of various water-soluble proteins entrapped in silica gels derived from alkoxysilane precursors.[12−15] Their work spurred the development of optimized, biocompatible techniques for a variety of water-soluble proteins. These techniques would later be applied toward liposome entrapment. One of the main techniques included the addition of glycerol and osmolytes, such as sugar, to alter protein hydration.[16,17] However, this approach did not address the problematic presence of high concentrations of alcohol that resulted from the hydrolysis reactions of alkoxysilane precursors. The presence of alcohols is especially

Received: June 25, 2014
Revised: July 24, 2014
Published: July 25, 2014

   dx.doi.org/10.1021/la5025058 | Langmuir 2014, 30, 9780–9788

detrimental to lipid bilayers, as sufficiently high concentrations will lead to alcohol significantly partitioning into the bilayer, causing it to interdigitate.[18] To address this, Brennan's group further pioneered the development of biocompatible sol−gel chemistries that consisted of modified alkoxysilane precursors bearing covalently attached sugar moieties and/or glycerol.[19,20] Depending on the specific precursor, the quantity of alcohol liberated during hydrolysis reactions was either greatly reduced or completely removed, and the additives were unable to leach from the gel.

In 2002, Besanger et al. examined the stability of 1,2-dipalmitoyl-*sn*-glycero-3-phosphatidylcholine (DPPC) liposomes within silica gels derived from three different precursors: an unmodified alkoxysilane (tetraethyl orthosilicate or TEOS), an alkoxysilane with covalently attached glycerol (diglycerylsilane or DGS), and sodium silicate (SS).[21] Their work demonstrated that the use of DGS- and SS-derived gels permitted the DPPC liposomes to exhibit phase transitions as they would in solution, while the use of TEOS-derived gels did not. Also, they depicted, via confocal fluorescence imaging, that the liposomes are capable of undergoing a variety of conformational changes once trapped inside of the gel, forming aggregates or bicelles. Though the DGS- and SS-derived silica gels seemed to work favorably at first, the DPPC liposomes eventually lost the ability to undergo phase transitions several days later. It was speculated that this was due to rupturing of the liposomes. Halder et al. would corroborate this theory in 2004 by examining the solvation dynamics of coumarin 480 inside of liposomes entrapped in silica gel.[22] Other analyses of liposome−silica interactions have elucidated that silica has a propensity for deforming liposomes, causing them to rupture and fuse to the surface.[23] Moreover, silica is actually a very common substrate for performing liposomal fusion to make supported lipid bilayers.[24−26]

An alternate approach for circumventing the problematic alcohol presence was presented in 2002 by Ferrer et al. It consisted of a simple technique where rotary evaporation was used prior to incorporation of biological species.[27] This approach was later utilized by Luo et al. in 2005 to entrap liposomes bearing the IMPs bacteriorhodopsin and ATP-synthase in silica gels derived from the precursor tetramethyl orthosilicate (TMOS).[28] Though protein activity was observed after entrapment, the condition of the liposomal hosts was not examined. On the basis of their analysis, it is unknown whether or not the protein was functioning near its optimal activity, if the liposomes retained their structure over time, or if this approach would work well for other biologically significant IMPs.

From these previous works, it can be seen that liposomes undergo structural changes and altered lipid dynamics upon entrapment; thus, they are not optimal biological membrane hosts for IMPs inside of silica gel. In addition, the size mismatch of liposomes (∼100−200 nm in solution) with mesoporous silica (5−50 nm pores) is a limiting factor in their successful implementation as biological membrane host for IMPs.[29] Here we look to improve upon the use of liposomes in silica gel by instead utilizing nanolipoprotein particles (NLPs) as biological membrane hosts. NLPs are discoidal patches of lipid bilayer associated with amphiphilic scaffold proteins that interact with the hydrophobic domain of the bilayer by wrapping around the particle periphery, making the entire structure water-soluble. NLPs have an average thickness of 5 nm, with a diameter ranging from 10 to 25 nm depending on the stoichiometric ratios and types of lipids and scaffold proteins being used.[30] This allows NLPs to be more compatible with the pore size (5−50 nm) of mesoporous silica and bear more resemblance to water-soluble proteins—the molecules for which this architecture was optimized—than liposomes. Therefore, here we perform entrapment of NLPs using a quick, simple sol−gel processing technique for TMOS that includes evaporation of the majority of the methanol after the hydrolysis reactions. The lipid phase behavior of entrapped NLPs in comparison to entrapped liposomes was observed using fluorescence anisotropy measurements, while the secondary structure of the scaffold protein was examined via circular dichroism spectroscopy. We found that liposomes exhibited more significant modulations in their phase behavior upon entrapment in silica gel than NLPs and that modulations caused by residual methanol for both liposomes and NLPs are relatively small. Also, the scaffold protein of NLPs maintained a conformation indicative of protein−lipid interactions, thus strongly suggesting that there were minimal alterations in structure for NLPs. Our results demonstrate that NLPs are more favorable for silica gel entrapment than liposomes.

MATERIALS AND METHODS

Materials. MSP is a His-tagged membrane scaffold protein (MSP1E3D1, Sigma-Aldrich, Inc), which is comprised of residues 56−243 of human apoA-I and a 22 amino acid N-terminal fusion containing the His tag, a spacer sequence, and the TEV protease site. Imidazole (≥99%), TMOS (≥99%), 1,6-diphenyl-1,3,5-hexatriene (DPH) (≥98%), ethanol (200 proof), sodium chloride (≥99%), methanol (≥99%), and sodium cholate (≥99%) were also purchased from Sigma-Aldrich, Inc. 1,2-Dipentadecanoyl-*sn*-glycero-3-phosphocholine (Di15:0PC) was purchased in chloroform (10 mg/mL concentration) from Avanti Polar Lipids, Inc. Ni−NTA agarose was purchased from 5 PRIME, Inc. The tris(hydroxymethyl)-aminomethane (MB grade) and hydrochloric acid (12.1 N) used to prepare a Tris-HCl buffer stock solution (500 mM, pH 7.5) were purchased from USB Corp. and Fisher Scientific International, Inc., respectively. All water used in these experiments was purified in a Barnstead Nanopure System (Barnstead Thermolyne, Dubuque, IA) with a resistivity ≥17.9 MΩ·cm.

Preparation of Di15:0PC Liposomes. For a single preparation, an appropriate aliquot of Di15:0PC was removed from the 10 mg/mL chloroform stock solution, placed into a glass conical vial, dried with nitrogen, and then placed under mild vacuum for at least 4 h to fully evaporate all of the chloroform. The lipid film was then rehydrated with a reconstitution buffer (20 mM Tris, 100 mM NaCl, pH 7.4) to a final lipid concentration of 2 mg/mL and heated to 80 °C for at least 5 min. After hydration and heating, the lipids were extruded through 100 nm pore membranes in an extruder (Avestin, Inc., Ottawa, Canada). Finally, a small fraction of the resulting liposome solution was used for size determination via a particle size analyzer (Brookhaven Instruments Corp., Holtsville, NY).

Preparation of Di15:0PC MSP NLPs. NLP batches were synthesized by first placing a stoichiometric excess (6 mg) of Di15:0PC in chloroform solution inside of a glass conical vial. The contents were first dried using nitrogen and then placed under mild vacuum for at least 4 h. Afterward, the dried lipid film was rehydrated and solubilized with a sodium cholate reconstitution buffer (40 mM sodium cholate, 20 mM Tris, 100 mM NaCl) and transferred to a plastic centrifuge tube, where it was allowed to further mix at room temperature (22 ± 1 °C) on a vortex mixer (Fischer Scientific, Hampton, NH) for 30 min. Next, 0.93 mg of His-tagged MSP was added to the centrifuge tube and allowed to incubate at room temperature and 300 rpm for 1 h. After incubation, the NLP reaction mixture was transferred to a 10 000 MWCO (molecular weight cutoff) dialysis filter (Thermo Scientific, Rockford, IL) and dialyzed against a reconstitution buffer (20 mM Tris, 100 mM NaCl) at 250× volume

dx.doi.org/10.1021/la5025058 | *Langmuir* 2014, 30, 9780−9788

excess to remove cholate. Dialysis was performed for 4 h at room temperature and 20 additional hours at 4 °C. Over the course of the 24 h dialysis, the buffer was exchanged three times (250^4 overall cholate dilution factor). After dialysis, the NLPs were purified using Ni−NTA agarose. The solution of His-tagged NLPs was incubated with Ni−NTA agarose at 4 °C for at least 2 h. The ratio of NLPs and Ni−NTA agarose was prepared such that the concentration of NLPs was far below the maximum binding capacity of the Ni−NTA agarose. After incubation, the agarose was separated via gentle centrifugation (500 rpm) and the supernatant aqueous phase was removed. Centrifugation was also used during the subsequent wash and elution steps to separate the agarose from the aqueous phase. The agarose was washed four times with a wash buffer (20 mM imidazole, 20 mM Tris, 100 mM NaCl). The agarose was then eluted four times with an elution buffer (400 mM imidazole, 20 mM Tris, 100 mM NaCl). The supernatant liquid removed after each elution was concentrated using 100 000 MWCO centrifugal concentrators (Vivaproducts, Inc. Littleton, MA) and combined for a total volume of roughly 1 mL. NLPs were then dialyzed again under the same conditions previously mentioned for the purpose of imidazole removal. The concentration of MSP was determined using a UV−vis spectrophotometer (Shimadzu Scientific Instruments, Columbia, MD) to measure the concentration of MSP via absorbance at 280 nm. The lipid concentration was determined by synthesizing a separate batch of NLPs using Di15:0PC that was laced with a trace amount of fluorescent Oregon Green 488 DHPE (Life Technologies, Carlsbad, CA) and using an Oregon Green standard curve to measure fluorescence intensities of the resulting NLP batch with a fluorescence spectrophotometer (PerkinElmer, Inc., Waltham, MA). The lipid to protein ratio (4 mg:1 mg) was consistent with the expected ratio of MSPs to lipids (2:375).[30] The size of the NLPs was measured using a particle size analyzer (Brookhaven Instruments Corp., Holtsville, NY). The acquired Stokes diameter was converted to a discoidal diameter using known thicknesses of phosphatidylcholine bilayers (see the Supporting Information).

Entrapment of Liposomes and NLPs in Silica Gel. For a typical preparation, 5.6 mL of 0.01 M HCl in nanopure water was combined with 7.6 mL of TMOS in a round-bottom flask and swirled until a uniform, cloudy phase was observed. The solution was then subjected to sonication in a bath sonicator for 10 min, followed by rotary evaporation (340 mbar reduced pressure, 50 °C) for 20 min to promote rapid removal of methanol liberated during the hydrolysis reactions. The solution was then passed through a 0.45μm filter, resulting in roughly 4 mL of a clear silica sol. Of the 4 mL of silica sol, 1 mL was placed into a methacrylate cuvette, followed by 1 mL of a stronger reconstitution buffer (34 mM Tris, 100 mM NaCl) in order to neutralize the pH. Afterward, 1 mL of either a 20× diluted liposome solution or 20× diluted NLP solution in regular reconstitution buffer (20 mM Tris, 100 mM NaCl) was added to the methacrylate cuvette. The liposome stock solution was typically 2.8 mM 15:0 PC (final concentration 56 μM inside gel), while the NLP stock solution was typically 20 μM MSP (final concentration 400 nM inside gel). Gelation typically occurred within 2 min after addition of the liposomes or NLPs.

Fluorescence Anisotropy Measurements. Ten microliters of a 100 μM DPH stock solution in ethanol was added to either liposome or NLP solutions in 1 mL volumes of reconstitution buffer (20 mM Tris, 100 mM NaCl). Afterward, these samples were either diluted further (3×) and used for solution anisotropy readings or added as the final 1 mL aliquot during the aforementioned entrapment/gelation process and used for gel anisotropy readings. Anisotropy values (r) are determined by the difference in polarized light intensity emitted parallel and perpendicular to the excitation source normalized by the total light intensity emitted, as shown in eq 1.[31]

$$r = \frac{I_{||} - I_{\perp}}{I_{||} + 2I_{\perp}} \tag{1}$$

The measurements were carried out on a PerkinElmer LS 55 fluorescence spectrometer equipped with a PTP-1 fluorescence Peltier system (PerkinElmer, Inc., Waltham, MA). A wavelength of 360 nm was used for excitation, while emission intensities at 440 nm were used for determining anisotropy values. Band passes of 3 and 5 nm were used on the excitation and emission monochromators, respectively. The anisotropy values were recorded at varying temperature intervals (≤4 °C) as temperature was raised at an average rate of 0.4 °C/min. Anisotropy values reported are the average of at least four measurements at a given temperature. Each sample was subjected to only one anisotropy heating cycle before disposal. Each sample was used to generate a single anisotropy plot. There were no fluorescence emissions at 440 nm (hence no anisotropy signals) from the silica gel, protein, or lipid; only DPH-containing samples showed fluorescence emission intensities.

Cooperativity and Melting Temperature Determination. The anisotropy vs temperature experimental data was regressed using the method of least-squares for an empirical phase transition model shown in eq 2, where the parameters r_{max}, r_{min}, T_m, and n are the maximum anisotropy, minimum anisotropy, melting temperature, and cooperativity index, respectively.[32]

$$r(T) = \frac{r_{max} - r_{min}}{1 + e^{(T-T_m)n}} + r_{min} + AT + BT^2 \tag{2}$$

A and B are constant coefficients for the quadratic baseline. Ignoring the quadratic baseline, eq 2 depicts a sigmoid function with asymptotic end behavior in the limit as T is significantly far from the phase transition region. The parameters r_{max} and r_{min} represent the vertical displacement of the plot, while T_m corresponds to the inflection point (for significantly small values of B) and n corresponds to the broadness of the phase transition region. A quadratic baseline can be used in the vicinity of the phase transition region to more accurately capture the manner in which anisotropy varies with temperature, as well as any asymmetry about the inflection point. The parameters A and B were chosen to be the average of all of the individually regressed data plots. This was due to a trade-off between n and the quadratic baseline during the regression process; A and B can influence the value of n. By fixing A and B, the change in n between different plots is almost entirely attributed to the sample, with minimal effect from other parameters. To implement this, each plot was regressed individually, while its values for A and B were recorded. Once all of the values were recorded and averaged, all of the plots were reregressed with fixed values for A and B (see the Supporting Information). These values were the overall average from the previous regressions.

Circular Dichroism Spectroscopy of NLPs. In order to perform circular dichroism (CD) spectroscopy, the 20 mM Tris, 100 mM NaCl buffer was replaced with a 25 mM Phosphate, 100 mM NaF buffer due to absorbance of Tris and chloride in the UV region of interest. Solution and gelated measurements were performed on a JASCO J-715 spectropolarimeter with a 2 cm/min scan speed (JASCO, Easton, MD). Data points were collected as averages of three scans from 260 to 190 nm at room temperature in a demountable close-ended far-UV (Q) 1 mm path length quartz cuvette cell type 20C (STARNA Cells) for the silica gel samples and in a 1 mm path length open-end quartz cuvette for the solution samples. The final concentrations of MSP were 20 μM in solution and 60 μM in silica gel.

Estimation of α-Helix Content from CD Spectra. The α-helical content was determined by first converting the measured ellipticity at 222 nm to a molar ellipticity using eq 3, where $[\theta]_{molar}$, MRW, θ_{222}, l, and c are the molar ellipticity (deg cm^2 dmol^{-1}), MSP mean residue weight (g/mol), ellipticity (deg), cuvette path length (cm), and MSP concentration (g/mL), respectively.

$$[\theta]_{molar} = (\mathrm{MRW} \times \theta_{222})/10lc \tag{3}$$

Once this was obtained, a common correlation[33] shown in eq 4 was used to estimate the percentage of α-helical content.

$$\%\alpha\text{-helix} = (-[\theta]_{molar} + 3000)/39000 \tag{4}$$

RESULTS

Fluorescence Anisotropy Measurements and Regressions. Fluorescence anisotropy of the membrane-inserting

dx.doi.org/10.1021/la5025058 | Langmuir 2014, 30, 9780−9788

probe 1,6-diphenyl-1,3,5-hexatriene (DPH) was used to investigate the phase behavior of Di15:0PC carbonyl tails within liposomes and NLPs. Di15:0PC was used instead of other biologically prevalent PC lipids (such as DMPC or DPPC) due to the compatibility of its phase transition temperature with the heating/cooling speeds of the Peltier element in the experimental setup, which allowed for higher throughput of samples in a given period of time (see the Supporting Information). Liposomes had a Stokes diameter of 166.5 ± 1.8 nm, while NLPs had a Stokes diameter of 11.7 ± 2.2 nm and corresponding discoidal diameter of 14.8 ± 4.4 nm by dynamic light scattering. We obtained fluorescence anisotropy values using eq 1 at a range of temperatures that included the main phase transition and in two environments, aqueous buffer solution and porous silica gel derived from the alkoxysilane precursor, TMOS. As shown in Figure 1A, the phase transition from a solid lipid phase to a liquid disordered lipid phase, observed as a decrease in anisotropy with increasing temperature, was broader for NLPs than that of the liposomes in buffer.

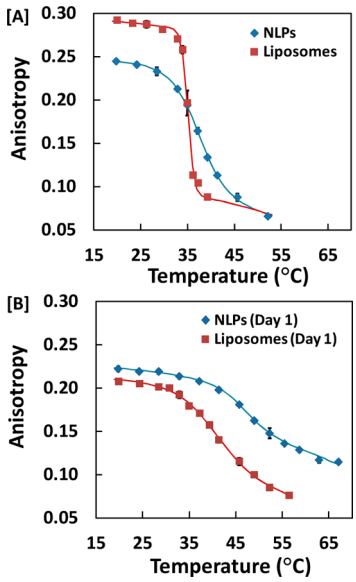

Figure 1. Measured anisotropy values of NLPs and liposomes in (A) 20 mM Tris, 100 nM NaCl buffer and (B) silica gel after initial entrapment, with corresponding regression curves as temperature was increased.

This corresponds to the disparity in the cooperativity indices (n) of the phase transition, obtained by fitting to eq 2. When lipid bilayers undergo a phase transition, the transition occurs involving multiple subunits known as cooperative units. The cooperativity index is a relative scale that is directly proportional to the size of the cooperative unit. The NLPs have an average index of 0.36 ± 0.20 and the liposomes have an average index of 1.79 ± 0.24, both in solution. Figure 1A also illustrates the shift in the midpoint of the phase transition (T_m) to higher temperature for NLPs in comparison to liposomes. By fitting this data to eq 2, T_m values are found to be 35.1 ± 0.1 and 37.7 ± 0.6 °C on average for the liposomes and NLPs, respectively. Immediately after entrapment in silica gel (day 1), phase transitions can be observed by the decrease in anisotropy with increasing temperature, as shown in Figure 1B. However, the anisotropy range—the overall ordinate axis difference between the maximum and minimum anisotropy values—was reduced for both NLPs and liposomes in comparison to solution anisotropy ranges. In addition, Figure 1 and Table 1 show that the T_m values of both NLPs and liposomes entrapped in silica gel are elevated compared to their solution values.

Table 1 illustrates that the cooperativity indices for NLPs and liposomes entrapped within silica gel were on the same order of magnitude, with the NLP values being slightly higher. These values were on the same order of magnitude of NLP cooperativity in solution, but were an order of magnitude lower than that of liposome cooperativity in solution. This is depicted in Figure 2A, where the cooperativity of NLPs and liposomes entrapped in silica gel are plotted over a 5−6 week period, normalized by their respective solution values.

The normalized cooperativity for NLPs started near unity and decayed to a constant value of approximately 0.7 over the course of 2 weeks (Figure 2A). The liposomes maintained a constant normalized cooperativity between 0.1 and 0.2 over the entire 5-6 week period (Figure 2A). In solution, cooperativity did not exhibit any significant changes over time for both NLPs and liposomes as it remained unaffected over the course of 3 weeks (see Tables S1 and S2, Supporting Information). In addition to the normalized cooperativity, the phase transition temperature (T_m) of liposomes entrapped within silica gel remained relatively constant in the 40−42 °C region over the course of the 5-6 week period, as shown in Figure 2B. The NLP T_m was higher, as it gradually increased and leveled off in the 46−50 °C region, as shown in Figure 2B. As with cooperativity, T_m also remained relatively unaffected in solution over the course of 3 weeks for both NLPs and liposomes (see Tables S1 and S2, Supporting Information). For all samples, the observed

Table 1. Selected Regression Parameters for Liposomes and NLPs under Various Conditions

	condition	T_m (°C)	n	$n_{normalized}$
NLPs	solution	37.7 ± 0.2	0.36 ± 0.03	1
	gel (no Rotovap, day 1)	40.0 ± 0.5	0.35 ± 0.05	0.98 ± 0.15
	gel (day 1)	46.3 ± 0.6	0.33 ± 0.06	0.93 ± 0.10
	gel (day 7)	47.9 ± 0.7	0.30 ± 0.05	0.85 ± 0.12
	gel (day 14)	48.2 ± 0.4	0.25 ± 0.02	0.72 ± 0.07
	gel (day 36)	49.5 ± 0.8	0.25 ± 0.05	0.72 ± 0.14
liposomes	solution	35.1 ± 0.1	1.79 ± 0.30	1
	gel (day 1)	41.3 ± 0.8	0.22 ± 0.03	0.12 ± 0.03
	gel (day 7)	42.1 ± 0.6	0.26 ± 0.02	0.13 ± 0.02
	gel (day 13)	41.8 ± 0.5	0.28 ± 0.03	0.14 ± 0.02
	gel (day 39)	40.4 ± 0.9	0.22 ± 0.03	0.14 ± 0.03

dx.doi.org/10.1021/la5025058 | Langmuir 2014, 30, 9780−9788

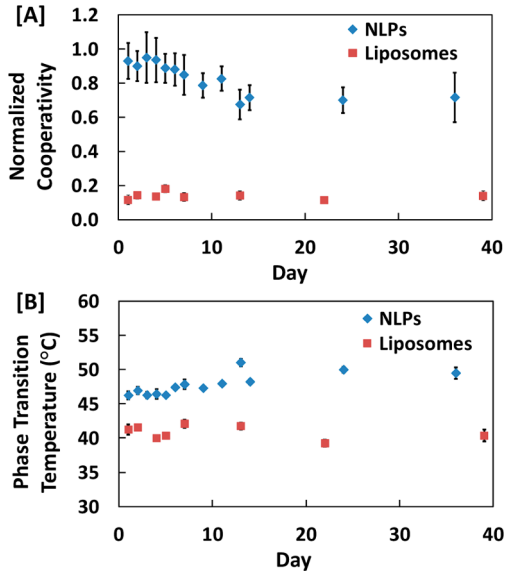

Figure 2. Regressed values for (A) cooperativity and (B) phase transition temperature of NLP and liposome samples entrapped in silica gel over the course of 5−6 weeks.

anisotropy curves were reversible with respect to temperature in solution. However, they were not reversible in silica gel and appeared somewhat broadened (data not shown). Therefore, different samples were independently aged and used to generate single sets of parameters. The plots in Figure 2 are the averaged scatter plots of the regressed values for 20 silica gels entrapping NLPs and 9 silica gels entrapping liposomes.

Upon synthesis of TMOS-derived silica gel, methanol was liberated and reduced using rotary evaporation. The methanol content in rotary evaporated silica was determined to be roughly 5 v/v%, while untreated silica had a methanol concentration of 24 v/v% (see the Supporting Information). Due to its presence, the effect of methanol on the phase behavior of Di15:0PC in NLPs and liposomes was examined. As shown in Figure 3, the anisotropy values of NLPs in buffer solution decreased in nearly constant intervals as the concentration of methanol was increased at all temperatures. This was also observed for liposomes (see Figure S3, Supporting Information).

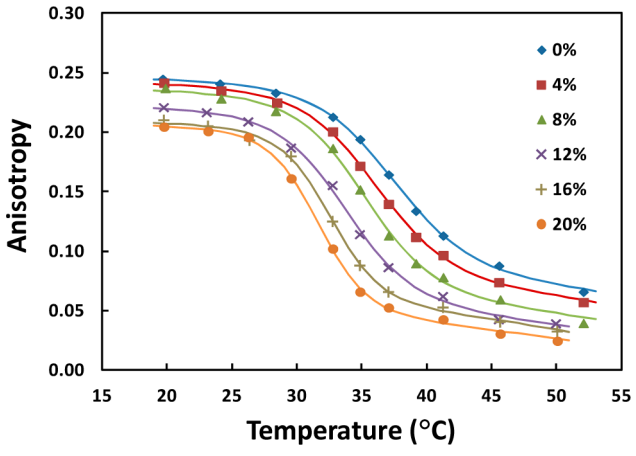

Figure 3. Measured anisotropy values and corresponding regression curves of different NLP samples in 20 mM Tris, 100 mM NaCl at various concentrations of methanol (v/v%).

Moreover, the T_m values for NLPs and liposomes monotonically decreased and then increased with increasing methanol concentration, as shown in Figure 4A, with minimum T_m values

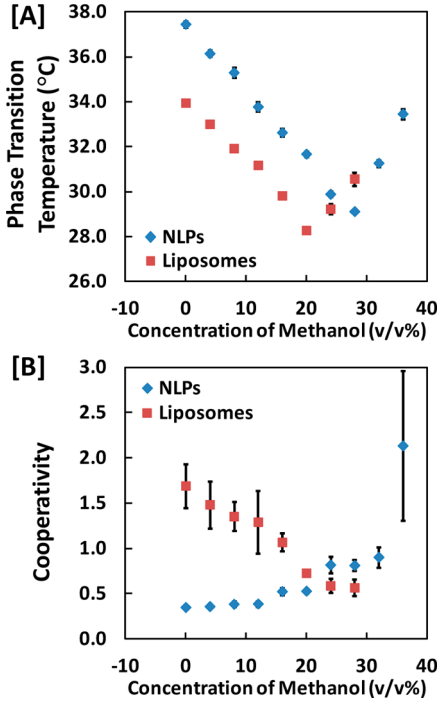

Figure 4. Regressed parameters for (A) phase transition temperature (T_m) and (B) cooperativity (n) of NLPs and liposomes in 20 mM Tris, 100 mM NaCl buffer in methanol−aqueous buffer solutions.

of 29.1 ± 0.1 °C at 28 ± 4 v/v% methanol and 28.3 ± 0.1 °C at 20 ± 4 v/v% methanol, respectively. Cooperativity indices, obtained by fits to eq 2, did not show corresponding minima or maxima and instead increased for NLPs and decreased for liposomes with increasing methanol concentration, as shown in Figure 4B

As the methanol concentration was increased in solution, the size of particles in NLP samples also increased. At 0, 15, and 30 v/v%, the Stokes diameter of particles in NLP solution samples was 11.7 ± 2.2, 17.3 ± 3.2, and 93.0 ± 3.5 nm, respectively (see Table S3, Supporting Information). The effect of methanol was also examined inside silica gel for NLPs, where samples without rotary evaporation during the sol−gel processing were compared to samples utilizing it. In Figure 5 and Table 1, it is shown that elimination of the rotary evaporation step, which

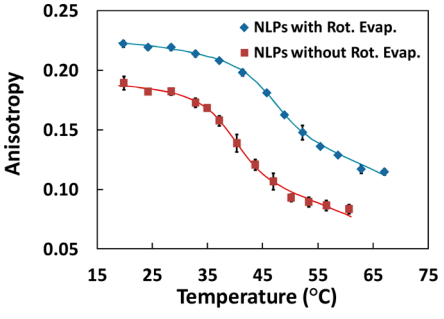

Figure 5. Measured anisotropy values of NLPs in silica gel after initial entrapment with and without the use of rotary evaporation during the sol−gel processing.

dx.doi.org/10.1021/la5025058 | Langmuir 2014, 30, 9780−9788

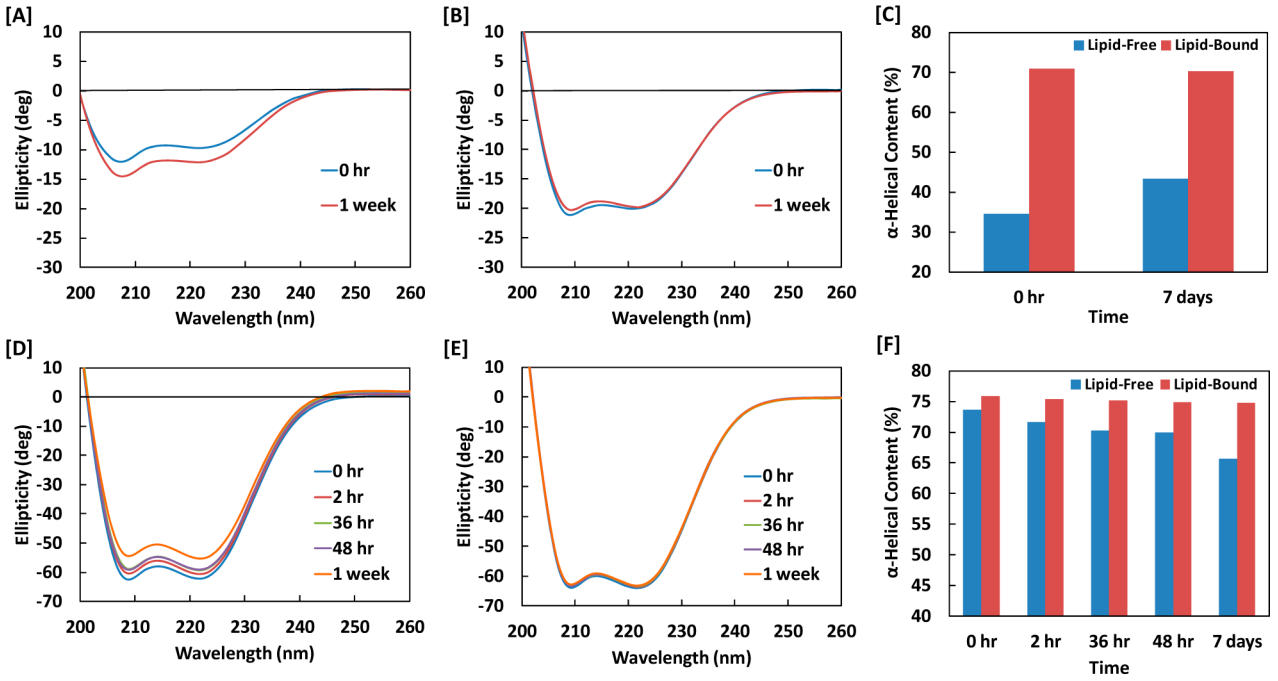

Figure 6. Circular dichroism spectra of (A) lipid-free MSP in solution and (B) lipid-bound MSP (NLPs) in solution and (C) corresponding solution α-helix content determined from 222 nm ellipticity. Circular dichroism spectra of (D) lipid-free MSP in silica gel and (E) lipid-bound MSP (NLPs) in silica gel, with (F) corresponding gel α-helix content.

corresponds to higher methanol concentrations, resulted in lowered anisotropy values and a reduced phase transition temperature (46.3 ± 0.6 °C for rotary evaporated samples and 40.0 ± 0.5 °C for non-rotary-evaporated samples). In addition, it was observed that the cooperativity change was small (0.33 ± 0.06 °C for rotary evaporated samples and 0.35 ± 0.05 °C for non-rotary-evaporated samples).

Circular Dichroism Spectra. Far-UV circular dichroism spectroscopy was used to examine the secondary structures of the scaffold protein MSP in lipid-free and lipid-bound conformations. Figure 6 shows spectra in terms of ellipticity vs wavelength for MSP alone (lipid-free) and MSP assembled in NLPs (lipid-bound) in both solution and gel-entrapped states. It can be seen that there were vertical shifts in spectral intensity for MSP over the course of 1 week. These shifts were more prominent for samples where MSP was in a lipid-free conformation (Figure 6A,D) in comparison to samples where it was in a lipid-bound conformation (Figure 6B,E) in both solution and silica gel, respectively.

For all CD spectra in Figure 6, two peaks characteristic of substantial α-helical content were evident (located at 208 and 222 nm[34]). The actual α-helical content was estimated from the 222 nm peak using eqs 3 and 4, as other secondary structural elements have little contribution to this region of a protein spectrum.[35] In Figure 6C, the α-helical content in buffer solution was shown to remain at 70% for lipid-bound MSP and increase from 35% to 43% for lipid-free MSP over the course of 1 week. In Figure 6F, the α-helical content in silica gel was shown to remain constant at 75% for lipid-bound MSP and decrease from 73% to 65% for lipid-free MSP over the course of 1 week.

DISCUSSION

Liposome and NLP Phase Behavior. Liposomes can contain tens to hundreds of thousands of lipids per structure and have cooperativity units that have been estimated to include up to 1700 lipid molecules.[36] Having fewer lipids per structure, NLPs are not capable of forming cooperative units as large as those present in liposomes. The NLPs used in this work contained roughly 375 lipids per disk. In addition, a fraction of the lipids, located in a two-lipid-thick belt along the scaffold protein boundary, undergo a concomitant loss of cooperativity after NLP formation.[37,38] Therefore, in solution, NLPs inherently have a lower cooperativity index than liposomes, as we have observed here. The presence of scaffold proteins has also been shown to elevate the phase transition temperature in solution, as observed here, for a given lipid incorporated into NLPs compared to when incorporated into liposomes due to an increase in lateral pressure from the protein−lipid interactions.[37]

Upon entrapment in the silica gel, cooperativity of the NLP phase transition decreased slightly (93% ± 10% of solution value) while cooperativity of the liposomes decreased significantly (12% ± 3% of solution value). This leads us to believe that the liposomes are undergoing significant structural changes upon entrapment, while the NLPs are not. A significant reduction in size of liposomes has been shown to result in lowered cooperativity.[39] The rupturing of liposomes and formation of smaller lipid aggregates or bicellar structures could reasonably explain this observed behavior and has previously been observed in other works where liposomes were entrapped in silica gel.[21,22] Moreover, only a slight reduction in cooperativity and elevation in phase transition temperature (compared to liposomes) for NLPs observed over the course of 5−6 weeks could indicate that they are not undergoing significant alterations in their size and structure after entrapment.

Upon silica gel entrapment, there was an observed elevation in phase transition temperature for NLPs and liposomes, which is consistent with previous work where elevated phase

dx.doi.org/10.1021/la5025058 | Langmuir 2014, 30, 9780−9788

transitions for entrapped liposomes were observed due to speculated excluded volume effects.[21] This is analogous to effects observed in work with thermal unfolding of proteins in silica gel, where a higher free energy (thus higher unfolding temperature) was imposed upon entrapped, folded proteins due to decreased volume available for the unfolded form.[40,41] Since the lipid tails become less dense when undergoing a gel phase to liquid crystalline transition,[42] it is reasonable to believe that the excluded volume effect can be involved. The observed decreased in anisotropy range is due either to a change in the packing and motion of the lipid tails in each phase or release of a portion of the DPH into the pores of the silica gel (see the Supporting Information). Nonetheless, a decrease in the anisotropy range does not have significant effect on the regressed values for the cooperativity index or phase transition temperature (see Figure S1, Supporting Information).

We speculate that the minor (approximately 20%) reduction in cooperativity over weeks for entrapped NLPs could be related to the known phenomenon of silica gel shrinkage over time.[20,43] Since phospholipid headgroups are known to interact strongly with silica surfaces,[23] changes in the geometry and size of pores could directly impact adsorbed NLPs. A decrease in size of lipid structure is correlated to a decrease in cooperativity and could rationalize this observation; however, the possibility of aggregation is not ruled out. A decrease in silica gel size corresponds to a decrease in porosity, which would enhance the excluded volume effect, explaining our observed increase in phase transition temperature over weeks for NLPs. Further work in analyzing different silane precursors and monolith shrinkage effects on lipid structures would be required to validate this hypothesis. Overall, these results make it very plausible that the silica sol−gel-entrapped NLPs, unlike liposomes, maintain a structure resembling their solution counterparts for weeks at a time.

Methanol Effects on NLP Phase Behavior. Due to the presence of residual methanol in the silica gels (∼5 v/v%), the effect of methanol on anisotropy values and phase behavior for NLPs and liposomes in solution was examined. The trend in decreasing anisotropy and minimum T_m values for NLPs and liposomes as the methanol concentration was increased is consistent with previous fluorescence anisotropy studies involving short-chain alcohols,[44] as well as similar studies in which lipid absorbance at 400 nm was utilized.[45,46] Short-chained alcohols increase the area per molecule of the lipid bilayer[47,48] and induce the interdigitated phase;[18] thus, the DPH probe is allowed to more freely rotate, lowering the anisotropy value. The minimum in the T_m value is reported to correspond to the completion of the interdigitation transition.[45,46] The elevation in methanol concentration required to fully interdigitate NLPs could indicate that they have a slightly higher resistance to bilayer interdigitation. The presence of the scaffold proteins could perhaps prolong the bilayer structure in elevated methanol concentrations due to direct interactions with the lipid tails, making it more difficult for them to interlace. The use of TMOS instead of the popular precursor TEOS is favorable due to its liberation of methanol, which requires exponentially higher concentrations than ethanol to significantly modulate lipid bilayer behavior.[48] We found that in the vicinity of 5 v/v% methanol, anisotropy and T_m values for NLPs and liposomes were minimally changed. Therefore, the more significant changes in these values for silica sol−gel-entrapped NLPs and liposomes were not caused by the presence of methanol.

While the liposomes display a decrease in the cooperativity index, cooperativity increases for NLPs with increasing methanol concentration. The interdigitated phase of bilayers tends to have a lower phase transition temperature than the gel phase;[18,45,46] thus, the decrease in the cooperativity that is observed is potentially the result of coexistence between the gel and interdigitated phases. This coexistence would result in the transition appearing broader, as the phase transition equation used (eq 2) only accounts for one inflection point. However, at 5 v/v% methanol, the cooperativity of the phase transition is only decreased by approximately 10% in comparison to 90% decrease observed for liposomes entrapped in silica gel. In the case of the NLPs, the measured increase in aggregate size in methanol solutions would account for larger cooperative units, which would directly increase the cooperativity index. The appearance of the opposite trend, i.e., slightly decreasing cooperativity, for silica-gel-entrapped NLPs illustrates that the methanol concentration is below the threshold necessary for aggregate growth.

By removing most of the methanol through rotary evaporation in silica sol−gel-entrapped NLPs, we have avoided significant changes in anisotropy and T_m caused by methanol. If we did not use rotary evaporation, the solution methanol concentration was roughly 24 v/v% with accompanying decreased anisotropy and T_m values, which were consistent in magnitude with what was observed in solution experiments. However, the increase in cooperativity was minimal compared to that observed in solution. The size of the pores (5−50 nm) could perhaps limit the NLPs from aggregating or remodeling into larger lipid structures that would have cooperative units comparable to those in solution.

Protein Conformational Changes in NLPs. The presence of α-helical secondary structure is essential for NLP formation and protein−lipid binding.[49] We found that the α-helical content of the scaffold protein MSP is significantly higher in its lipid-bound NLP-associated state (70%), versus a lipid-free state (35%−43%) in solution. This magnitude of difference is consistent with previous works that examined α-helical content in very similar scaffold proteins, such as MSP1D1[50] and apolipoprotein A-I.[49,51,52] For apolipoprotein A-I, this is due to 4 of the 10 helical regions forming a bundle in the lipid-free state, while the other 6 helical regions, along with the globular region, fold in a variety of different conformations having relatively higher random coil content.[53] It is reasonable to believe that similar behavior is involved for MSP, as it is derived directly from apolipoprotein A-I. Once entrapped in silica gel the α-helical content of MSP in NLP samples increased slightly to 75%. Interestingly, entrapped MSP in its lipid-free state adopted a significantly higher α-helical content than in solution, increasing to 73%. These results are consistent with previous discoveries of the biocompatible environment of silica sol−gels for water-soluble proteins which are often stabilized against denaturation and aggregation in silica sol−gels. The stabilization effect has been attributed to the ability of the sol−gel matrix to restrict conformational flexibility and diffusional motion and to promote structural rigidity in the water environment.[54,55] The confinement from the pores of the silica gel could rationalize the observed increase in α-helical content for MSP upon entrapment; an estimated radius of gyration of 3 nm for randomly structured MSP in solution (see the Supporting Information) is on the same order of magnitude as the pore size. This could potentially cause MSP to adopt an alternative conformation that consists of higher α-helical

dx.doi.org/10.1021/la5025058 | Langmuir 2014, 30, 9780−9788

content. The decrease of α-helical content over the course of a week (73%−65%) for lipid-free MSP in silica gel in comparison to the steady α-helical content of 75% for lipid-bound MSP could indicate that the silica gel promotes lipid association of MSP, thereby maintaining the higher helical conformation of this state.[49,56] However, the absence of lipids does not allow MSP to maintain a constant conformation.

CONCLUSIONS

We have demonstrated that nanolipoprotein particles (NLPs) are more compatible with the nanoscale environment of the silica gel pores in comparison to liposomes. Direct measurement of size of soft matter inside of mesoporous silica is difficult to obtain; thus, we utilized biophysical characterization in the form of fluorescence anisotropy and circular dichroism spectroscopy to directly investigate lipid phase behavior and scaffold protein secondary structure, as well as indirectly correlate this behavior to aggregate size. Fluorescence anisotropy, which is then used to analyze the cooperativity and temperature of the main phase transition, revealed that NLPs entrapped in silica gel exhibit phase behavior with a stronger resemblance to their solution counterparts than liposomes. In particular, cooperativity indices indicate that entrapment in silica gel causes immediate large-scale changes in lipid aggregation state of liposomes toward smaller cooperative units and only minor changes for NLPs over weeks of time. These large-scale changes in liposomes have been linked in the past to liposome rupture and denaturation of integral membrane proteins. By investigating these same properties for liposomes and NLPs in methanol solutions, we find that the small amount of methanol remaining after evaporative removal is not sufficient to cause observed changes in these properties upon sol−gel entrapment. However, if we did not remove the methanol, we found that entrapped NLPs displayed shifts in anisotropy and phase transition temperature that were consistent with large fractions of methanol but that the cooperativity was relatively maintained, which we attribute to limitations in the growth of the NLPs by confinement in the nanoporous environment of the silica gel. Upon further investigation of conformational changes, circular dichroism revealed that the scaffold protein of the entrapped NLPs maintained a consistent α-helical content necessary for its structural function of belting the phospholipids. This is consistent with the known biocompatibility and structure promotion of silica gels for water-soluble proteins. Future work will entail the incorporation of integral membrane proteins inside of NLPs and analysis/quantification of their activity retention upon sol−gel-derived entrapment via protein-specific assays.

ASSOCIATED CONTENT

Supporting Information

Detailed methods, calculations, and figures. This material is available free of charge via the Internet at http://pubs.acs.org.

AUTHOR INFORMATION

Corresponding Author

*E-mail: mllongo@ucdavis.edu.

Notes

The authors declare no competing financial interest.

ACKNOWLEDGMENTS

The project described was supported by Grant Number T32-GM008799 from NIGMS-NIH. Its contents are solely the responsibility of the authors and do not necessarily represent the official views of the NIGMS or NIH. Contributions by A.N.P. and access to fluorescence spectrophotometer are supported by a grant from Basic Energy Sciences, U.S. DOE (# DE-FG02-04ER46173).

REFERENCES

(1) Avnir, D.; Coradin, T.; Lev, O.; Livage, J. Recent Bio-Applications of Sol−Gel Materials. *J. Mater. Chem.* **2006**, *16* (11), 1013−1030.
(2) Nassif, N.; Livage, J. From Diatoms to Silica-Based Biohybrids. *Chem. Soc. Rev.* **2011**, *40* (2), 849−59.
(3) Ruiz-Hitzky, E.; Ariga, K.; Lvov, Y. *Bio-Inorganic Hybrid Nanomaterials: Strategies, Syntheses, Characterization and Applications*; WILEY-VCH: Weinheim, Germany, 2008.
(4) Gill, I. Bio-Doped Nanocomposite Polymers: Sol−Gel Bioencapsulates. *Chem. Mater.* **2001**, *13* (10), 3404−3421.
(5) Brennan, J. D. Biofriendly Sol−Gel Processing for Entrapment of Soluble and Membrane-Bound Proteins: Toward Novel Solid-Phase Assays for High-Throughput Screening. *Acc. Chem. Res.* **2007**, *40* (9), 827−835.
(6) Kato, M.; Sakai-Kato, K.; Toyo'oka, T. Silica Sol−Gel Monolithic Materials and Their Use in a Variety of Applications. *J. Sep. Sci.* **2005**, 1893−1908.
(7) Monton, M. R. N.; Forsberg, E. M.; Brennan, J. D. Tailoring Sol−Gel Derived Silica Materials for Optical Biosensing. *Chem. Mater.* **2012**, *24* (5), 796−811.
(8) Avdulov, N. A.; Chochina, S. V.; Draski, L. J.; Deitrich, R. A.; Wood, W. G. Chronic Ethanol Consumption Alters Effects of Ethanol in Vitro on Brain Membrane Structure of High Alcohol Sensnity and Low Alcohol Sensitivity Rats. *Alcohol.: Clin. Exp. Res.* **1995**, *19* (4), 886−891.
(9) Lu, J. Z.; Huang, F.; Chen, J. W. The Behaviors of Ca^{2+} ATPase Embedded in Interdigitated Bilayer. *J. Biochem.* **1999**, *126* (2), 302−306.
(10) Lucero, P.; Penalver, E.; Monero, E.; Lagunas, R. Moderate Concentrations of Ethanol Inhibit Endocytosis of the Yeast Maltose Transporter. *Appl. Environ. Microbiol.* **1997**, *63* (10), 3831−3836.
(11) Mitchell, D. C.; Lawrence, J. T. R.; Litman, B. J. Primary Alcohols Modulate the Activation of the G Protein-Coupled Recepter Rhodopsin by a Lipid-Mediated Mechanism. *J. Biol. Chem.* **1996**, *271* (32), 19033−19036.
(12) Flora, K. K.; Brennan, J. D. Effect of Matrix Aging on the Behaviour of Human Serum Albumin Entrapped in a Tetraethylorthosilicate-Derived Glass. *Chem. Mater.* **2001**, *13* (11), 4170−4179.
(13) Baker, G. A.; Jordan, J. D.; Bright, F. V. Effects of Poly(ethylene glycol) Doping on the Behavior of Pyrene, Rhodamine 6g, and Acrylodan-Labeled Bovine Serum Albumin Sequestered within Tetramethylorthosilane-Derived Sol−Gel-Processed Composites. *J. Sol−Gel Sci. Technol.* **1998**, *11* (1), 43−54.
(14) Gottfried, D. S.; Kagan, A.; Hoffman, B. M.; Friedman, J. M. Impeded Rotation of a Protein in a Sol−Gel Matrix. *J. Phys. Chem. B* **1999**, *103* (14), 2803−2807.
(15) Shen, C.; Kostic, N. M. Kinetics of Photoinduced Electron Transfer Reactions within Sol−Gel Silica Glass Doped with Zinc Cytochrome *c*. *J. Am. Chem. Soc.* **1997**, *119* (6), 1304−1312.
(16) Eggers, D. K.; Valentine, J. S. Crowding and Hydration Effects on Protein Conformation: A Study with Sol−Gel Encapsulated Proteins. *J. Mol. Biol.* **2001**, *314* (4), 922−922.
(17) Brennan, J. D.; Benjamin, D.; Dibattista, E.; Gulcev, M. D. Using Sugar and Amino Acid Additives To Stabilize Enzymes within Sol−Gel Derived Silica. *Chem. Mater.* **2003**, *15* (3), 737−745.
(18) Slater, J. L.; Huang, C. Interdigitated Bilayer Membranes. *Prog. Lipid Res.* **1988**, *27* (4), 325−359.

(19) Chen, Y.; Zhang, Z.; Sui, X. H.; Brennan, J. D. Reduced Shrinkage of Sol−Gel Derived Silicas Using Sugar-Based Silsequioxane Precursors. *J. Mater. Chem.* **2005**, *15* (30), 3132−3141.
(20) Brook, M. A.; Chen, Y.; Guo, K.; Zhang, Z.; Brennan, J. D. Sugar-Modified Silanes: Precursors for Silica Monoliths. *J. Mater. Chem.* **2004**, *14* (9), 1469−1479.
(21) Besanger, T.; Zhang, Y.; Brennan, J. D. Characterization of Fluorescent Phospholipid Liposomes Entrapped in Sol−Gel Derived Silica. *J. Phys. Chem. B* **2002**, *106* (41), 10535−10542.
(22) Halder, A.; Sen, S.; Burman, A. D.; Patra, A.; Bhattacharyya, K. Solvation Dynamics of Dimyrsistoyl-Phosphatidylcholine Entrapped inside a Sol−Gel Matrix. *J. Phys. Chem. B* **2004**, *108* (7), 2309−2312.
(23) Reimhault, E.; Hook, F.; Kasemo, B. Intact Vesicle Adsorption and Supported Biomembrane Formation from Vesicles in Solution: Influence of Surface Chemistry, Vesicle Size, Temperature, and Osmotic Pressure. *Langmuir* **2003**, *19* (5), 1681−1691.
(24) Reimhault, E.; Zach, M.; Hook, F.; Kasemo, B. A Multitechnique Study of Liposome Adsorption on Au and Lipid Bilayer Formation on SiO_2. *Langmuir* **2006**, *22* (7), 3313−3319.
(25) Tero, R.; Takizawa, M.; Li, Y.; Yamazaki, M.; Urisu, T. Lipid Membrane Formation by Vesicle Fusion on Silicon Dioxide Surfaces Modified with Alkyl Self-Assembled Monolayer Islands. *Langmuir* **2004**, *20* (18), 7526−7531.
(26) Jing, Y.; Trefna, H.; Persson, M.; Kasemo, B.; Svedhem, S. Formation of Supported Lipid Bilayers on Silica: Relation to Lipid Phase Transition Temperature and Liposome Size. *Soft Matter* **2014**, *10* (1), 187−195.
(27) Ferrer, M.; Del Monte, F.; Levy, D. A Novel and Simple Alcohol Free Sol Gel Route for Encapsulation of Labile Proteins. *Chem. Mater.* **2002**, *14* (9), 3619−3621.
(28) Luo, T. J.; Soong, R.; Lan, E.; Dunn, B.; Montemagno, C. Photo-Induced Proton Gradients and ATP Biosynthesis Produced by Vesicles Encapsulated in a Silica Matrix. *Nat. Mater.* **2005**, *4* (3), 220−224.
(29) Besanger, T.; Easwaramoorthy, B.; Brennan, J. D. Entrapment of Highly Active Membrane Bound Receptors in Macroporous Silica. *Anal. Chem.* **2004**, *76* (21), 6470−6475.
(30) Bricarello, D. A.; Smilowitz, J. T.; Zivkovic, A. M.; German, J. B.; Parikh, A. N. Reconstituted Lipoprotein: A Versatile Class of Biologically-Inspired Nanostructures. *ACS Nano* **2011**, *5* (1), 42−57.
(31) Lakowicz, J. *Principles of Fluorescence Spectroscopy*; Springer: New York, 2006.
(32) Nelson, S. C.; Neeley, S. K.; Melonakos, E. D.; Bell, J. D.; Busath, D. D. Fluorescence Anisotropy of Diphenylhexatriene and its Cationic Trimethylamino Derivative in Liquid Dipalmitoylphosphatidylcholine Liposomes: Opposing Responses to Isoflurane. *BMC Biophys.* **2012**, *5* (1), 5.
(33) Morrow, J. A.; Segall, M. L.; Lund-Katz, S.; Phillips, M. C.; Knapp, M.; Rupp, B.; Weisgraber, K. H. Differences in Stability among the Human Apolipoprotein E Isoforms Determined by the Amino-Terminal Domain. *Biochemistry* **2000**, *39* (8), 11657−11666.
(34) Kelly, S. M.; Jess, T. J. How To Study Proteins by Circular Dichrosim. *Biochim. Biophys. Acta* **2005**, *1751* (2), 119−139.
(35) Hirst, J. D.; Brooks, C. L. Helicity, Circular Dichroism and Molecular Dynamics of Proteins. *J. Mol. Biol.* **1994**, *243* (2), 173−178.
(36) Knoll, W. Calorimetric Investigations of Lipid Phase Transitions. I. The Width of Transition. *Thermochim. Acta* **1984**, *77* (1), 35−47.
(37) Denisov, I. G.; McLean, M. A.; Shaw, A. W.; Grinkova, Y. V.; Sligar, S. G. Thermotropic Phase Transition in Soluble Nanoscale Lipid Bilayers. *J. Phys. Chem. B* **2005**, *109* (32), 15580−15588.
(38) Shaw, A. W.; McLean, M. A.; Sligar, S. G. Phospholipid Phase Transitions in Homogeneous Nanometer Scale Bilayer Discs. *FEBS Lett.* **2004**, *556* (1), 260−264.
(39) Marsh, D.; Watts, A.; Knowles, P. F. Cooperativity of the Phase Transition in Single- and Multibilayer Lipid Vesicles. *Biochim. Biophys. Acta* **1977**, *465* (3), 500−514.
(40) Eggers, D. K.; Valentine, J. S. Molecular Confinement Influences Protein Structure and Enhances Thermal Protein Stability. *Protein Sci.* **2001**, *10* (2), 250−261.
(41) Zhou, H.; Dill, K. Stabilization of Proteins in Confined Spaces. *Biochemistry* **2001**, *40* (38), 11289−11293.
(42) Xie, A. F.; Yamada, R.; Gewirth, A. A.; Granick, S. Materials Science of the Gel to Fluid Phase Transition in a Supported Phospholipid Bilayer. *Phys. Rev. Lett.* **2002**, *89* (24), 246103.
(43) Brinker, C. J.; Scherer, G. W. *Sol-Gel Science: The Physics and Chemistry of Sol-Gel Processing*; Academic Press: San Diego, CA, 1990.
(44) Kim, Y. H.; Higuchi, W. I.; Herron, J. N.; Abraham, W. Fluorescence Anisotorpy Studies on the Interaction of the Short Chain *n*-Alkanols with Stratum Corneum Lipid Liposomes (SCLL) and Distearoylphosphatidylcholine (DSPC)/Distearoylphosphatidic Acid (DSPA) Liposomes. *Biochem. Biophys. Acta, Biomembr.* **1993**, *1148* (1), 139−151.
(45) Rowe, E. S. Thermodynamic Reversibility of Phase Transitions. Specific Effects of Alcohols on Phosphatidylcholines. *Biochem. Biophys. Acta, Biomembr.* **1985**, *813* (2), 321−330.
(46) Koynova, R.; Caffrey, M. Phases and Phase Transitions of the Phosphatidylcholines. *Biochim. Biophys. Acta, Rev. Biomembr.* **1998**, *1376* (1), 91−145.
(47) Ly, H. V.; Block, D. E.; Longo, M. L. Interfacial Tension Effect of Ethanol on Lipid Bilayer Rigidity, Stability, and Area/Molecule: A Micropipet Asipiration Approach. *Langmuir* **2002**, *18* (23), 8988.
(48) Ly, H. V.; Longo, M. L. The Influence of Short-Chain Alcohols on Interfacial Tension, Mechanical Properties, Area/Molecule, and Permeability of Fluid Lipid Bilayers. *Biophys. J.* **2004**, *87* (2), 1013−33.
(49) Saito, H.; Dhanasekaran, P.; Nguyen, D.; Deridder, E.; Holvoet, P.; Lund-Katz, S.; Phillips, M. C. α-Helix Formation Is Required for High Affinity Binding of Human Apolipoprotein A-I to Lipids. *J. Biol. Chem.* **2004**, *279* (20), 20974−20981.
(50) Morgan, C. R.; Hebling, C. M.; Rand, K. D.; Stafford, D. W.; Jorgenson, J. W.; Engen, J. R. Conformational Transitions in the Membrane Scaffold Protein of Phospholipid Bilayer Nanodiscs. *Mol. Cell. Proteomics* **2011**, *10* (9), M111−010876.
(51) Alexander, E. T.; Tanaka, M.; Kono, M.; Saito, H.; Rader, D. J.; Phillips, M. C. Structural and Functional Consequences of the Milano Mutation (R173c) in Human Apolipoprotein AI. *J. Lipid Res.* **2009**, *50* (7), 1409−1419.
(52) Petrlova, J.; Dalla-Riva, J.; Mörgelin, M.; Lindahl, M.; Krupinska, E.; Stenkula, K. G.; Voss, J. C.; Lagerstedt, J. O. Secondary Structure Changes in ApoA-I Milano (R173C) Are Not Accompanied by a Decrease in Protein Stability or Solubility. *PloS One* **2014**, *9* (4), e96150.
(53) Pollard, R. D.; Fulp, B.; Samuel, M. P.; Sorci-Thomas, M. G.; Thomas, M. J. The Conformation of Lipid-Free Human Apolipoprotein A-I in Solution. *Biochemistry* **2013**, *52* (52), 9470−81.
(54) Zheng, L.; Brennan, J. D. Measurement of Intrinsic Fluorescence To Probe the Conformational Flexibility and Thermodynamic Stability of a Single Tryptophan Protein Entrapped in a Sol−Gel Derived Glass Matrix. *Analyst* **1998**, *123* (8), 1735−1744.
(55) Das, T. K.; Khan, I.; Rousseau, D. L.; Friedman, J. M. Preservation of the Native Structure in Myoglobin at Low pH by Sol−Gel Encapsulation. *J. Am. Chem. Soc.* **1998**, *120* (39), 10268−10269.
(56) Nolte, R. T.; Atkinson, D. Conformational Analysis of Apolipoprotein A-I and E-3 Based on Primary Sequence and Circular Dichroism. *Biophys. J.* **1992**, *63* (5), 1221−1239.